ISSN 1990-7931, Russian Journal of Physical Chemistry B, 2022, Vol. 16, No. 4, pp. 787–796. © Pleiades Publishing, Ltd., 2022.

CHEMICAL PHYSICS OF NANOMATERIALS

Preparation of Magnesium Aluminate Spinel Nanofibers with High Temperature Resistance by Electrospinning Process Based on Non-Hydrolytic Sol-Gel Method

K. Xu[a], Yi. Cui[a, b, *], Y. Yu[b], H. Wei[a, b, **], H. Wang[a], Y. Wei[a], Y. Chen[a], D. Lv[a], Y. Yu[b], and J. Bu[a]

[a] *College of Materials Science and Engineering, Hebei Provincial Key Laboratory of Inorganic Nonmetallic Materials, North China University of Science and Technology, Tangshan, Hebei, 063009 China*

[b] *Key Laboratory of Inorganic Coating Materials, Chinese Academy of Sciences, Shanghai, 200050 China*

**e-mail: cuiyi870322@163.com*

***e-mail: why_why2000@163.com*

Received August 30, 2021; revised October 12, 2021; accepted October 20, 2021

Abstract—The magnesium aluminum spinel nanofibers are prepared by non-hydrolytic sol-gel and electrospinning methods using $MgCl_2$ and $AlCl_3$ as raw materials and PVP as spinning aid. The formation process of magnesium aluminum spinel nanofibers and the effect of calcination temperatures on the nanofibers are explored. The results show that magnesium chloride alkoxide and aluminum chloride alkoxide are formed after the addition of $AlCl_3$ and $MgCl_2$ into EtOH, respectively. The Mg–O–Al gel network is formed by the non-hydrolytic condensation reaction between the metal chloride alkoxides. The precursor fibers are synthetized using the electrospinning process. After calcination at 600°C, the nanofibers with magnesium aluminum spinel phase can be obtained and their average diameter is about 240 nm. When the precursor fibers are calcined at 1000 and 1300°C, the fibers are still continuous, smooth, and their diameter distribution is uniform. When the precursor fibers are subjected to the calcination temperature of 1600°C, the samples still maintain fibrous structure although the surface of fibers is rough. It indicates that the magnesium aluminum spinel nanofibers have excellent high temperature resistance.

Keywords: $MgAl_2O_4$ fiber, electrospinning, non-hydrolytic sol-gel method, high temperature resistance

DOI: 10.1134/S1990793122040054

INTRODUCTION

Magnesium aluminum spinel ($MgAl_2O_4$) is the only crystalline compound in the $MgO–Al_2O_3$ binary system. It has the advantages of high melting point (2135°C), hardness (16 GPa) and mechanical strength (135–216 MPa), low thermal expansion coefficient (9×10^{-6}/°C, 30–1400°C) and thermal conductivity (5.4 W m^{-1} K^{-1}, 1200°C), good thermal shock resistance and corrosion resistance, excellent infrared transmission and insulation, and chemical stability [1–4]. In addition, magnesium aluminum spinel fibers also have the outstanding characteristics of low density, high operating temperature (up to 1700–2000°C), high elastic modulus, high temperature oxidation resistance and creep resistance. For these reasons, as a novel type of refractory material, magnesium aluminum spinel fibers can be used as insulation material for aerospace aircraft and heat insulation of kilns [5–7]. On the other hand, it also has a wide range of applications in microelectronics, precision optical devices, catalyst carriers and fiber-reinforced materials applications.

Magnesium aluminum spinel fibers are usually prepared by the pulling and extrusion process, aerodynamic spraying and melt spinning method [8–14]. For example, magnesium aluminum spinel fibers were prepared by pulling and extrusion process using aluminum chlorohydrex, anhydrous magnesium chloride, aluminum tri(sec-butoxide) and magnesium acetate hydrate as raw materials, respectively [8, 9]. Magnesium aluminate spinel fibers were also obtained from a fiber-forming precursor based on aluminum and magnesium polycarboxylates by means of aerodynamic spraying method [10]. The $MgAl_2O_4$ fibers prepared through the above methods are mostly micron in diameter, which are inflexible and damage easily.

Recently, electrospinning method, as a versatile and viable technique for generating ceramic nanofibers, has received more and more attention. It is found that the fibers prepared by electrospinning process often have nano-scale fiber diameter, large aspect ratio and outstanding flexibility [15–19]. With regards to this, the $MgAl_2O_4$ nanofibers with porous and hollow structure were successfully synthesized by electrospinning method, which could be used in optical and

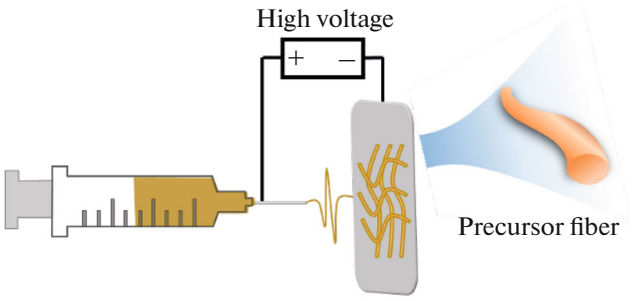

Fig. 1. Schematic illustration of electrospinning apparatus.

environmental purification applications [5, 20, 21]. Up now, the high temperature resistance of magnesium aluminum spinel nanofibers is still not investigated although $MgAl_2O_4$ fibers have potential in refractory field.

Besides that, precursor solution synthesis is a key step in preparing ceramic nanofibers by electrospinning process [22]. When inorganic metal salt sol is directly used for electrospinning, it is difficult to accurately control the rheological properties of inorganic sol. The spinning solution can also be obtained by introducing metal alkoxides. However, the rapid gelation of alkoxides during electrospinning process will lead to uneven fiber diameter and even blockage of nozzle. The adverse effect is often reduced by adding catalyst to adjust the hydrolysis polymerization rate of metal alkoxides. Moreover, the non-hydrolytic sol-gel method is based on the non-hydrolytic condensation reaction between metal halides and oxygen donors, rather than the hydrolysis and polymerization process of conventional metal alkoxides. It is not only simple and easy to achieve atom-scale uniform, but also the residual organic groups on surface of non-hydrolytic gel can help the gel dissolve in organic solvents [23, 24]. Therefore, non-hydrolytic sol-gel process have been used in electrospinning method for the preparation of ceramic nanofibers, such as mullite and forsterite nanofibers [25, 26].

Herein, magnesium aluminum spinel gel precursor fibers were prepared by non-hydrolytic sol-gel method combined with electrospinning technology. The sol-gel formation process of magnesium aluminum spinel gel and their transformation into spinel fibers were studied by FT-IR, DTA-TG-MS, XRD and TEM. And the high temperature resistance of magnesium aluminum spinel fibers was also investigated.

EXPERIMENTAL

Firstly, 0.5 mL ethanol (EtOH, CH_3CH_2OH) was dropped into 15 mL dichloromethane (CH_2Cl_2), then 0.14 g anhydrous magnesium chloride ($MgCl_2$) and 0.40 g anhydrous aluminum chloride ($AlCl_3$) were added while stirring to obtain the mixture. The mixture was heated in the oven from room temperature to 110°C until the magnesium aluminum spinel gel was formed. 0.5 g polyvinyl pyrrolidone (PVP, Mw = 1 300000) was dissolved in 8 mL ethanol, stirred evenly and poured into the spinel gel. Then 1 mL N,N-dimethylformamide (DMF) and 2 mL ethanol were added to obtain the precursor solution. The schematic illustration of the electrospinning apparatus is shown in Fig. 1. Electrospinning parameters: voltage 15 kV, feed rate 0.8 mL/h, receiving distance 13 cm. The precursor fibers prepared by electrospinning were dried at 110°C for 16 h, and then calcined at different temperatures for 1 h, with heating rate of 3°C/min.

SAMPLES CHARACTERIZATION

The chemical structures of sol, gel and fiber were tested by Fourier transform infrared spectrometer (FTIR Spectrometer, VERTEX70, Germany). The differential thermal analysis-thermogravimetry-mass spectrometry (DTA-TG-MS, NETZSCH STA 449F5, Germany) of magnesium aluminum spinel gel and the gel/PVP precursor fiber were carried out. The phase composition of the product was analyzed by the X-ray diffractometer (XRD, D/MAX2500PC, Rigaku, Japan), The microstructure of the synthetic fibers was observed by the scanning electron microscope (SEM, S-4800, Japan) and transmission electron microscope (TEM, JEM-2010, Japan).

RESULTS AND DISCUSSION

In order to study the formation process of magnesium aluminum gel prepared by non-hydrolytic sol-gel method, Fig. 2 shows the infrared spectra of EtOH solution, $MgCl_2$ + EtOH solution, $AlCl_3$ + $MgCl_2$ + EtOH solution and gel, respectively. It can be seen that the strong and wide absorption band in the range of 3500–3200 cm^{-1}, and the band of 700–600 cm^{-1} corresponds to the bending vibration of the O–H bond of ethanol molecule. Due to the stretching vibration of C–O bond in ethanol, the absorption bands appear at 1068, 1030 and 870 cm^{-1}. The band in the range of 1500–1200 and 2880 cm^{-1} corresponds to the vibration of organic groups CH_2 and CH_3 [27]. When $MgCl_2$ was added into ethanol, the vibration peak of O–H bond (3500–3200 cm^{-1}) became weak, and the corresponding vibration peak of O–H bond in the range of 700–600 cm^{-1} shifted to low wavenumber and weakened, and the C–O bond vibration peaks of 1068, 1030 and 880 cm^{-1} also occurred some change in peak shape. In addition, the absorption bands at 1630 and 1420 cm^{-1} were more obvious. At the same time, a new characteristic absorption band belonging to Mg–O bond appeared at 621 cm^{-1}. This indicates that a weak C–(O–Mg) band was formed by substitution reaction of $MgCl_2$ and EtOH [28, 29]. After the addition of $AlCl_3$, the vibration peak of O–H bond and C–O

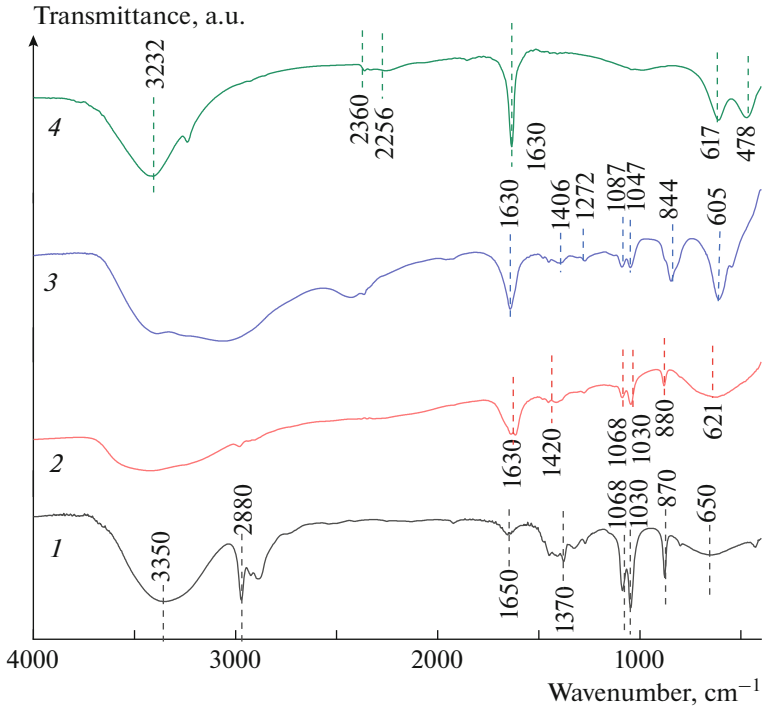

Fig. 2. FT-IR spectra of: (*1*) EtOH, (*2*) $MgCl_2$ + EtOH, (*3*) $AlCl_3$ + $MgCl_2$ + EtOH and (*4*) Gel.

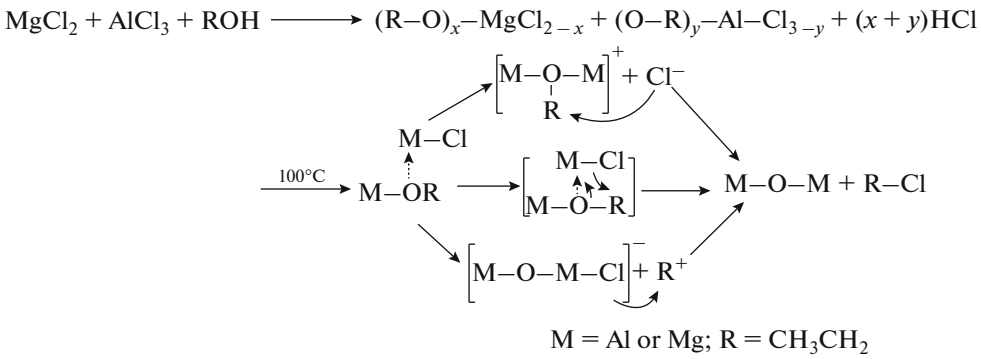

Fig. 3. Schematic diagram of gel formation process.

bond in the FT-IR spectra of the product became further weakened. The vibration peaks of C–(O–Al) and Al–Cl bond were observed at 605 and 844 cm^{-1}. It can be seen that magnesium chloride and aluminum chloride reacted with anhydrous ethanol to form magnesium chloride alkoxide and aluminum chloride alkoxide, respectively. In the FT-IR spectra of the gel, there are obvious vibration bands at 2360 and 2256 cm^{-1}, which are C–H vibration peaks in the gel, and Mg–O–Al stretching vibration absorption peaks appear at 617 and 478 cm^{-1}. This indicates that magnesium aluminum spinel gel network had been formed in the gel, and the gel process through the non-hydrolytic polymerization was shown in Fig. 3. The magnesium chloride alkoxide $(R–O)_x–MgCl_{2-x}$ and aluminum chloride alkoxide $(O–R)_y–AlCl_{3-y}$ were formed after adding $MgCl_2$ and $AlCl_3$ into ethanol, respectively. After the mixture was heat treatment at 110°C, Mg–O–Al gel was further formed though the non-hydrolytic substitution polymerization reaction [30–32].

The mass spectrometer coupled to the thermobalance was used to study the phase transformation of magnesium aluminum spinel gel/PVP precursor fibers and the gases formed during the heat treatment. The TG, DTG and DTA curves are presented in Fig. 4a of the curves *1–3*, respectively, while the evolved gas analysis by MS curves is shown in Fig. 4b. On the TG curve, three mass loss events are observed. From room

temperature to 250°C, the weight loss of the sample is 28% corresponds to the escape of CH_4 (m/z = 16), H_2O (m/z = 18), N_2 (m/z = 28), which may be due to the pyrolysis of residual organic matter, loss of adsorbed water and nitrogen on the surface of the precursor fibers [33–35]. The next two events occurred between 350–500°C with weight loss of 51.9%. These events can be attributed to the gradual pyrolysis of PVP and thermal degradation of the residual groups in the gel, which can be proved by the appearance of H_2O (m/z = 18), CO (m/z = 28), C_2H_4 (m/z = 28), NO (m/z = 30), HCl (m/z = 36), C_3H_7 (m/z = 43), CO_2 (m/z = 44), etc. [36–39]. In addition, the exothermic peak between 500 and 600°C is also related to the formation of spinel and the combustion of organic matter.

Figure 5 is the FT-IR spectra of PVP, precursor fiber and the fibers obtained at different calcination temperatures. It can be seen from the infrared spectra that the wide absorption band between 3000 and 3500 cm^{-1} is the H–O vibration peak of PVP. The peaks at 1430 and 1290 cm^{-1} are C–C and C–N vibrations on the ring skeleton, respectively. The absorption peak at 1660 cm^{-1} is C=O vibration absorption peak in PVP. The stretching vibration peak of C=O in PVP is located at 1650 cm^{-1} in the infrared spectrum of precursor fiber, indicating that the chemical bond between spinel gel and PVP is formed. With the increase of calcination temperature, the above absorption bands gradually weakened. With the calcination temperature of 500°C, the absorption bands in this spectrum gradually appear at 500–1000 cm^{-1} would correspond to the Mg–O–Al bond. When the calcination temperature is 600°C, two vibration peaks appear near 513 and 700 cm^{-1} which are the stretching vibration peaks of Al–O in octahedron [AlO_6] in magnesium aluminate spinel crystal structure, indicating that magnesium aluminum spinel phase has been formed after calcination at 600°C for 1 h [31]. When the calcination temperature increases to 700 and 900°C, the symmetry of these absorption bands is better, become more sharp and larger, suggesting the formation of spinel phase is more complete.

In order to study the effect of calcined temperature on magnesium aluminate spinel fibers, the precursor fibers were calcined at 500, 600, 700 and 900°C for 1 h, and the XRD pattern of the samples are shown in Fig. 6. It can be seen that when the fibers are calcined at 500°C, the XRD curve is basically a wide amorphous peak, and the product is still amorphous. The characteristic diffraction peak of magnesium aluminate spinel phase appeared in the XRD pattern of the samples obtained at 600, 700 and 900°C, corresponding to the JCPDS card (PDF#21-1152). The crystallinity index (CI) of the sample can be calculated according to Eq. (1) [40]

$$CI = \frac{A_c}{A_c + A_a}, \quad (1)$$

where A_c is the area under crystalline peaks and A_a is the area of amorphous hollows. When the calcination temperature is 600°C, the crystallinity index of the fiber is 86.91%. With the increase of calcination temperature, the polycrystalline structure gradually becomes perfect. The reflection of fibers calcined at 700 and 900°C is stronger than that of the fibers calcined at 600°C. These effects also indicate smaller coherent scattering regions and a less perfect crystalline structure when calcined at 600°C [12]. Compared with the traditional methods such as solid phase method and precipitation method, the complete $MgAl_2O_4$ phase need to be obtained above 1000°C. However, the $MgAl_2O_4$ phase will be formed when the fibers are calcined at 600°C, which significantly reduce the energy consumption of the technology.

SEM images of the fibers obtained at different calcination temperatures are shown in Fig. 7. It can be observed that the fibers have high continuity, large aspect ratio and smooth with no visible defects. The diameter of fibers changed with calcination temperatures improved. The diameter of precursor fibers is mainly distributed in 350–500 nm. After heat treatment at 500°C, the organic matter in the precursor fiber is volatilized after calcination, and the fibers' diameter becomes smaller. After heat treatment at 600 and 700°C, the fibers diameter is concentrated at about 240 and 200 nm, respectively. After heat treatment at 900°C, the average diameter of fibers is 187 nm, meanwhile the fibers diameter further decreased and the fibers' diameter is distributed in 100–250 nm.

In order to observe the internal structure of magnesium aluminate spinel nanofibers, TEM is used to analyze the nanofibers calcined at 900°C and the results are shown in Fig. 8. It can be seen that the fibers are composed of nanoparticles and their diameter is about 170 nm in Fig. 8a. Figure 8b shows that the SAED diffraction spots are periodically arranged concentric rings, indicating that the fiber is polycrystalline structure. The diffraction rings correspond to (111), (220), (311), (400), (511) and (440) crystal planes of $MgAl_2O_4$, respectively.

In order to further explore the high temperature resistance of magnesium aluminum spinel nanofibers, the sample is calcined at higher temperatures. Figure 9 shows the XRD patterns of magnesium aluminum spinel fibers calcined at 1000, 1300 and 1600°C. The results show that the main crystalline phases of the calcined samples are cubic magnesium aluminum spinel phase (PDF#21-1152), and their diffraction peaks correspond to (111), (220), (311), (400), (422), (511), (440) and (533) crystal planes, respectively, indicating that high temperature treatment has no effect on the fiber phase. When the calcination temperature increased to 1600°C, the diffraction peak intensity is further enhanced, and the magnesium aluminum spinel crystal is better developed. This is due to the formation of the second stage of spinel.

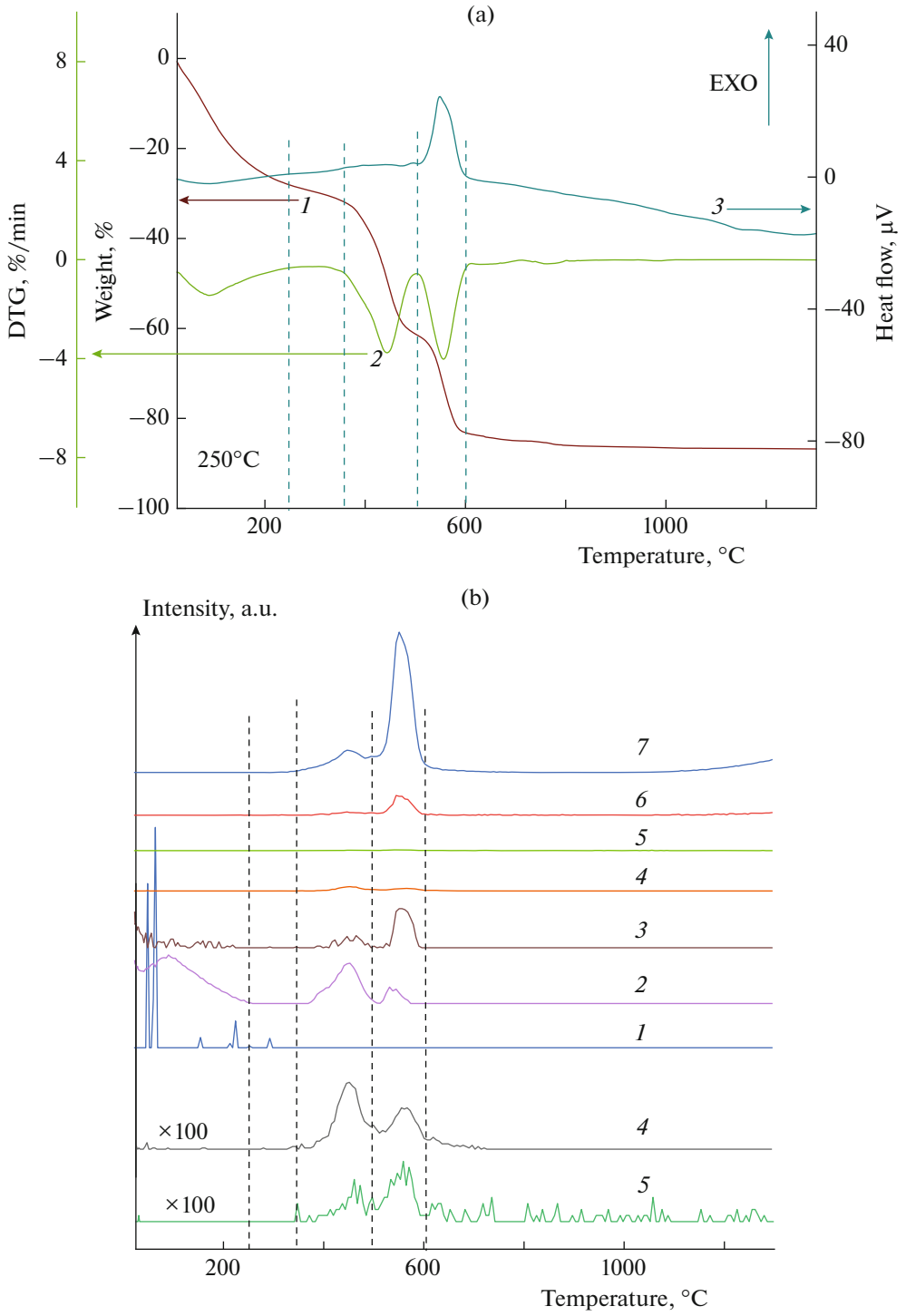

Fig. 4. (a) Thermogravimetric and differential thermal analysis ((*1*) TG, (*2*) DTG, (*3*) DTA); (b) continuous mass spectrometry of the gases (m/z = (*1*) 16, (*2*) 18, (*3*) 28, (*4*) 30, (*5*) 36, (*6*) 43, (*7*) 44) evolved during the heat treatment in air of magnesium aluminate spinel gels/PVP precursor fibers.

Figure 10 shows the SEM images and diameter distribution of the samples after higher temperature calcination. And the average diameter and diameter distribution of the fibers are shown in Table 1. The fibers randomly distributed and entangled with each other. It is found that when the calcination temperature is 1000°C, the fibers perform high continuity, smooth and non-crosslinking. When the calcination temperature is 1300°C, the average diameter of the fibers increases to 185 nm, and the fiber surface is uneven.

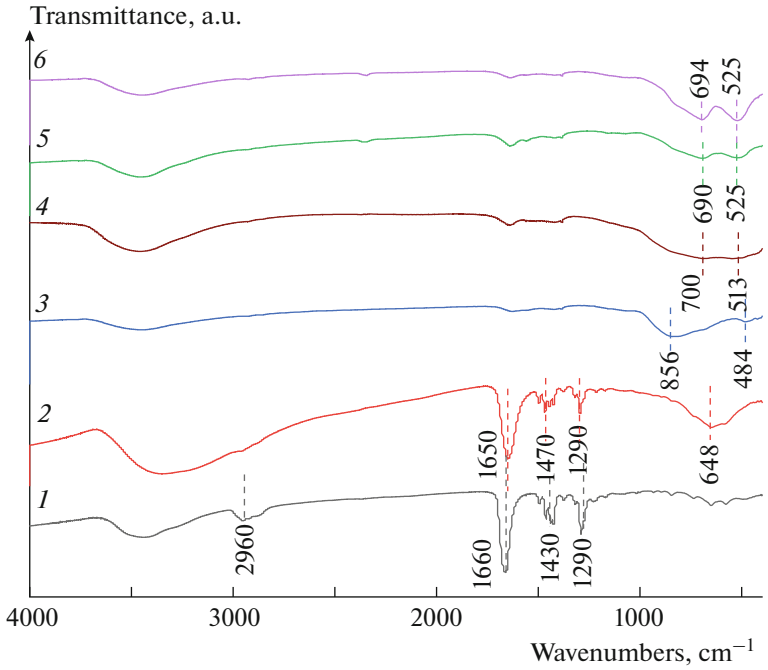

Fig. 5. FT-IR spectra of: (*1*) PVP, (*2*) precursor fiber, and fiber calcined at different temperature, (*3*) 500, (*4*) 600, (*5*) 700, (*6*) 900°C.

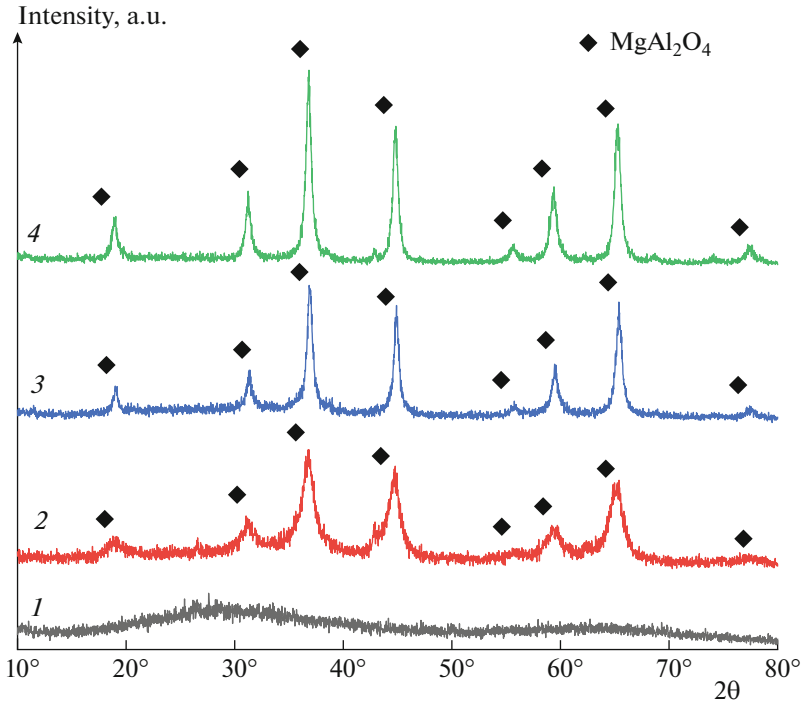

Fig. 6. XRD patterns of fibers calcined at different temperature for 1 h: (*1*) 500, (*2*) 600, (*3*) 700, (*4*) 500°C.

When the calcination temperature is increased to 1600°C, the fibers' surface becomes rough, and the grains on the spinel fiber developed well. Some fibers show uneven thickness, which may be due to the volumetric diffusion and the fact that small grains are gradually engulfed by larger grains, forming a chain structure.

In order to observe the microstructure of the nanofibers, Fig. 11 shows TEM images of the nanofiber calcined at 1600°C. The magnesium aluminate spinel

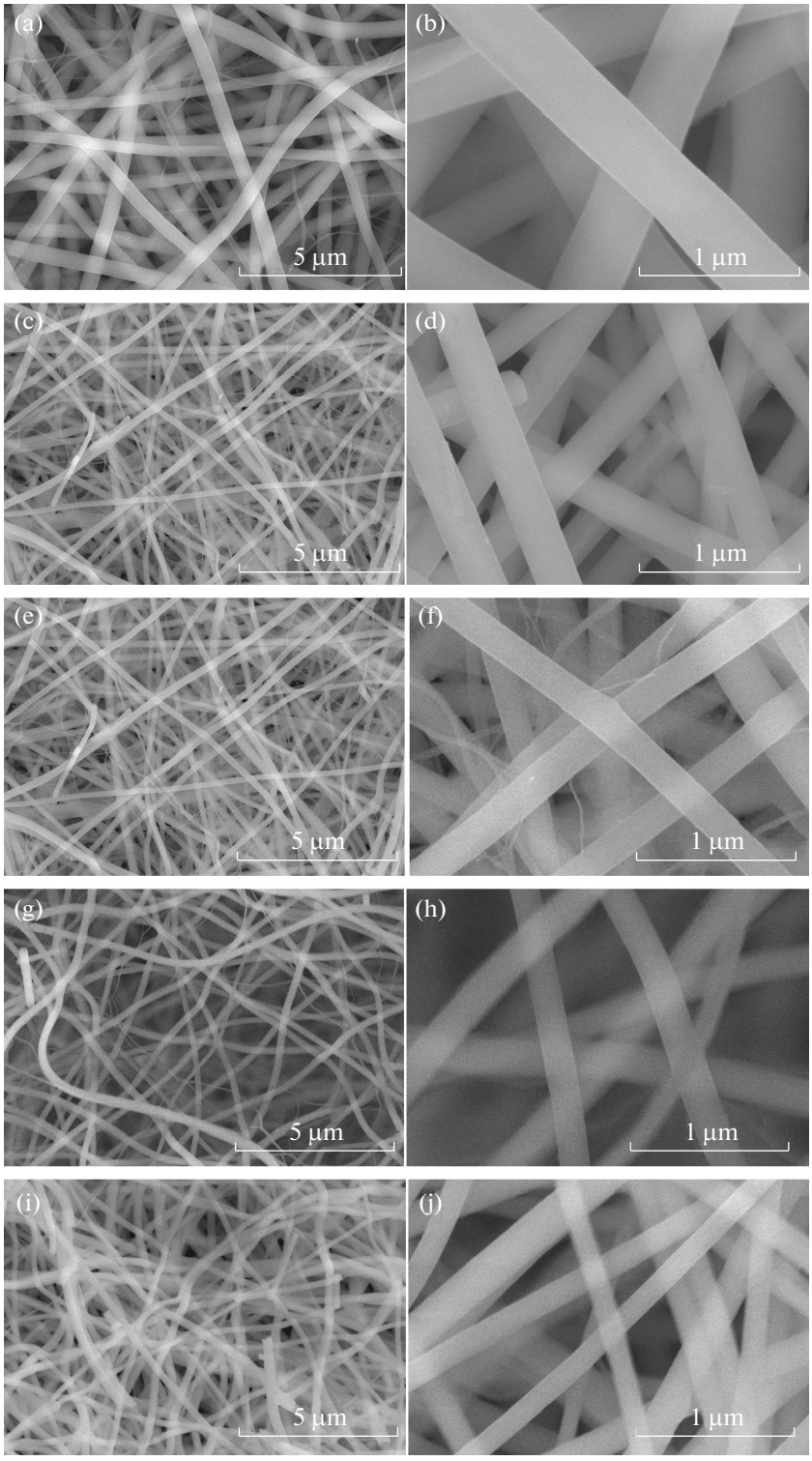

Fig. 7. SEM images of (a, b) precursor fiber without calcination and magnesium aluminate spinel fiber obtained at different temperatures: (c, d) 500; (e, f) 600; (g, h) 700; (i, j) 900°C.

crystal in the fiber is well developed, the particles size becomes larger and the grain boundary become obvious. The fibers' surface becomes rough, but the sample still maintained the fibrous morphology, which is similar with the SEM images. The SAED pattern confirms that the fiber is polycrystalline structure and the crystal is well developed. The diffraction rings correspond to (311), (400), (422), (511), (440) and (444)

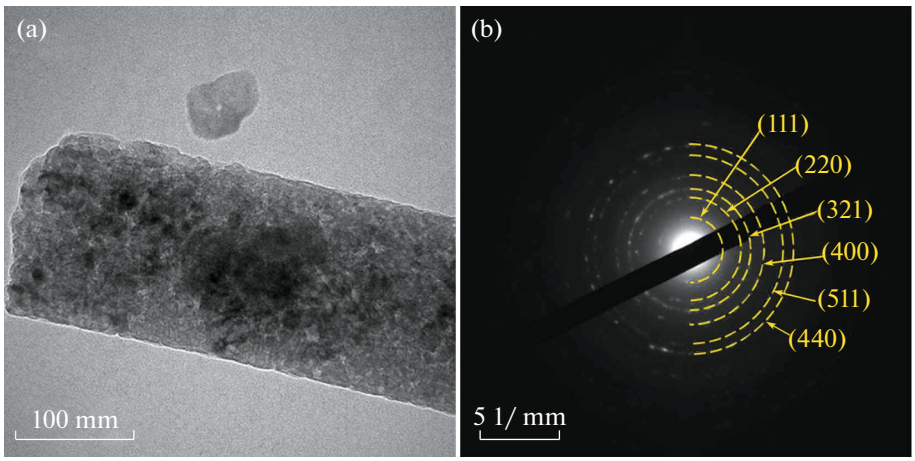

Fig. 8. TEM images and SAED images of magnesium aluminate spinel fiber calcined at 900°C.

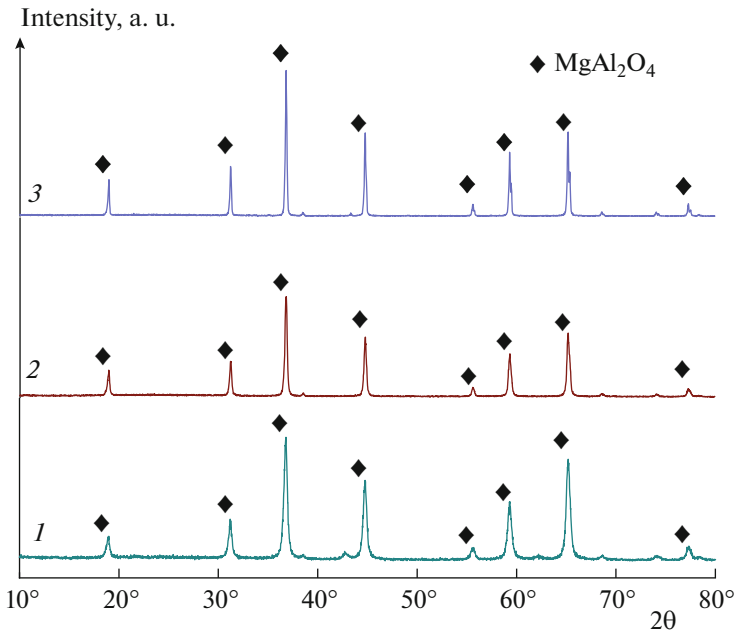

Fig. 9. XRD patterns of magnesium aluminate spinel fiber at different calcination temperatures: (*1*) 1000, (*2*) 1300, (*3*) 1600°C.

Table 1. Characterization of the fiber at different calcination temperatures

Calcination temperatures, °C	Diameter distribution, nm	Average diameter, nm
1000	50–250	130
1300	150–250	185
1600	160–200	150

crystal planes of magnesium aluminate spinel, respectively. This indicates that the magnesium aluminate spinel fibers prepared by electrospinning have high temperature resistance.

CONCLUSIONS

In this paper, magnesium aluminate spinel fibers were prepared by non-hydrolytic sol-gel process combined with electrospinning method, and the formation process of fibers and their high temperature resistance were investigated. Magnesium aluminate spinel fibers can be obtained after calcination at 600°C. The nano-

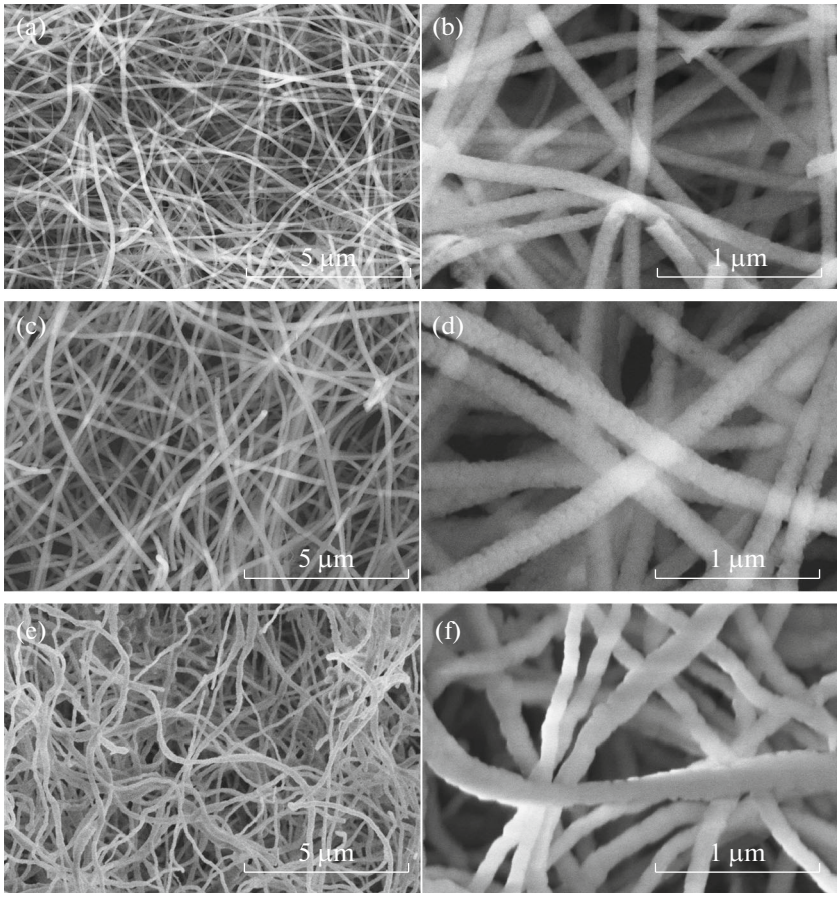

Fig. 10. SEM images of magnesium aluminate spinel fiber: (a, b) 1000; (c, d) 1300; (e, f) 1600°C.

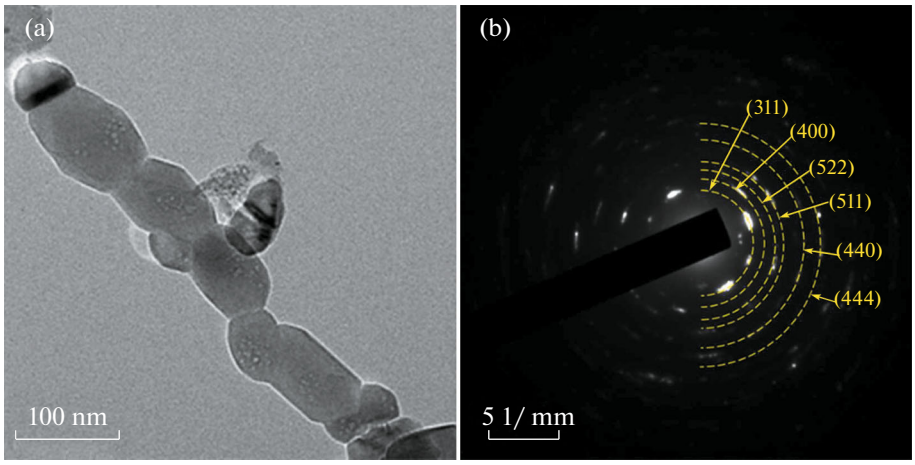

Fig. 11. TEM images (a) and SAED images (b) of magnesium aluminate spinel fiber calcined at 1600°C.

fibous morphology still maintained after calcination at 1600°C, indicating the nanofibers own outstanding high temperature resistance.

FUNDING

The research was supported by the National Natural Science Foundation of China (51302064 and 51472072), Outstanding Young Fund of North China University of Science and Technology (JQ201712), Hebei Natural Science Foundation (grant numbers E2021209120) and the Opening Project of Key Laboratory of Inorganic Coating Materials, Chinese Academy of Sciences (ICM-202006).

CONFLICT OF INTEREST

The authors declare that they have no conflicts of interest.

REFERENCES

1. I. Ganesh, Int. Mater. Rev. **58**, 63 (2013). https://doi.org/10.1179/1743280412Y.0000000001
2. Y. J. Kwon, H. G. Na, S. S. Kim, et al., Met. Mater. Int. **21**, 956 (2015). https://doi.org/10.1007/s12540-015-4443-5
3. V. M. Sreekumar, R. M. Pillai, B. C. Pai, et al., Appl. Phys. A **90**, 745 (2008). https://doi.org/10.1007/s00339-007-4357-2
4. H. Shafiee, A. Salehirad, and A. Samimi, Appl. Phys. A **126**, 198 (2020). https://doi.org/10.1007/s00339-020-3369-z
5. G. P. Dong, X. D. Xiao, M. Y. Peng, et al., RSC Adv. **2**, 2773 (2012). https://doi.org/10.1039/C2RA00516F
6. T. Zhang, Y. M. Zhou, X. H. Bu, et al., Ceram. Int. **41**, 12504 (2015). https://doi.org/10.1016/j.ceramint.2015.05.130
7. D. Y. Yang, F. L. Qian, K. Zhu, et al., Key Eng. Mater. **368**, 409 (2008). https://doi.org/10.4028/www.scientific.net/KEM.368-372.409
8. J. M. Boulton, K. Jones, and H. G. Emblem, J. Mater. Sci. Lett. **9**, 914 (1990). https://doi.org/10.1007/BF00722169
9. Y. Liu and R. M. Laine, J. Eur. Ceram. Soc. **19**, 1949 (1999). https://doi.org/10.1016/S0955-2219(99)00018-7
10. Y. A. Balinova, G. Y. Lyulyukina, and S. G. Kolyshev, Glass Ceram. **76**, 302 (2019). https://doi.org/10.1007/s10717-019-00188-1
11. W. C. Zhou and T. D. Mcgee, J. Mater. Sci. Lett. **17**, 673 (1998). https://doi.org/10.1023/A:1006628509142
12. T. M. Uljanova, L. V. Titova, N. P. Krut'ko, et al., Mech. Compos. Mater. **35**, 345 (1999). https://doi.org/10.1007/BF02259724
13. G. I. Shcherbakova, P. A. Storozhenko, T. L. Apukhtina, et al., J. Phys.: Conf. Ser. **1347**, 012049 (2019). https://doi.org/10.1088/1742-6596/1347/1/012049
14. W. Glaubitt, W. Watzka, H. Scholz, et al., J. Sol-Gel Sci. Technol. **8**, 29 (1997). https://doi.org/10.1007/BF02436813
15. Y. Q. Dai, W. Y. Liu, E. Formo, et al., Polym. Adv. Technol. **22**, 326 (2011). https://doi.org/10.1002/pat.1839
16. Z. Y. Li and C. Wang, *One-Dimensional Nanostructures Electrospinning Technique and Unique Nanofibers* (Springer, Berlin, 2013). https://doi.org/10.1007/978-3-642-36427-3
17. A. A. Ol'khov, O. V. Staroverova, M. A. Gol'dshtrakh, A. V. Khvatov, K. Z. Gumargalieva, and A. L. Iordanskii, Russ. J. Phys. Chem. B **10**, 830 (2016). https://doi.org/10.1134/S1990793116050213
18. A. A. Ol'khov, Y. V. Tertyshnaya, A. S. Chizhov, S. G. Karpova, and A. L. Iordanskii, Russ. J. Phys. Chem. B **12**, 293 (2018). https://doi.org/10.1134/S1990793118020227
19. S. G. Karpova, A. A. Ol'khov, P. M. Tyubaeva, N. G. Shilkina, A. A. Popov, and A. L. Iordanskii, Russ. J. Phys. Chem. B **13**, 313 (2019). https://doi.org/10.1134/S1990793119020039
20. R. Nakhowong, S. Kiennork, P. Wongwanwattana, et al., Mater. Lett. **220**, 234 (2018). https://doi.org/10.1016/j.matlet.2018.03.024
21. W. L. Ji, H. Y. Wei, H. Li, et al., J. Ceram. Soc. Jpn. **126**, 128 (2018). https://doi.org/10.2109/jcersj2.17123
22. J. J. Xue, T. Wu, Y. Q. Dai, et al., Chem. Rev. **119**, 5298 (2019). https://doi.org/10.1021/acs.chemrev.8b00593
23. P. H. Mutin and A. Vioux, Chem. Mater. **21**, 582 (2009). https://doi.org/10.1021/cm802348c
24. P. H. Mutin and A. Vioux, J. Mater. Chem. A **1**, 11504 (2013). https://doi.org/10.1039/C3TA12058A
25. H. Y. Wei, H. Li, Y. Cui, et al., J. Sol-Gel Sci. Technol. **82**, 718 (2017). https://doi.org/10.1007/s10971-017-4354-7
26. W. L. Ji, H. Y. Wei, Y. Cui, et al., Mater. Lett. **211**, 319 (2018). https://doi.org/10.1016/j.matlet.2017.09.118
27. B. H. Stuart, *Infrared Spectroscopy Fundamentals and Applications* (Wiley, New York, 2004). https://doi.org/10.1002/0470011149
28. D. C. Bradley, *Metal Alkoxides* (Academic, London, 1960). https://doi.org/10.1002/9780470166031.ch7
29. N. Y. Turova, E. P. Turevskaya, V. G. Kessler, et al., *The Chemistry of Metal Alkoxides* (Springer, Boston, 2002). https://doi.org/10.1007/b113856
30. Z. Mosayebi, M. Rezaei, N. Hadian, et al., Mater. Res. Bull. **47**, 2154 (2012). https://doi.org/10.1016/j.materresbull.2012.06.010
31. A. K. Adka, S. K. Saha, P. Pramanik, et al., J. Mater. Sci. Lett. **16**, 234 (1997). https://doi.org/10.1023/A:1018512025919
32. L. Z. Pei, W. Y. Yin, J. F. Wang, et al., Mater. Res. **13**, 339 (2010). https://doi.org/10.1590/S1516-14392010000300010
33. I. M. Szilágyi, E. Santala, M. Heikkilä, et al., J. Therm. Anal. Calorim. **105**, 73 (2011). https://doi.org/10.1007/s10973-011-1631-5
34. L. Bourget, R. J. P. Corriu, D. Leclercq, et al., J. Non-Cryst. Solids **242**, 81 (1998). https://doi.org/10.1016/S0022-3093(98)00789-3
35. G. S. Grader, G. E. Shter, and Y. D. Hazan, J. Mater. Res. **14**, 14 (1999). https://doi.org/10.1557/JMR.1999.0199
36. S. Acosta, R. Corriu, D. Leclercq, et al., J. Sol-Gel Sci. Technol. **2**, 25 (1994). https://doi.org/10.1007/BF00486208
37. O. Kéri, P. Bárdos, S. Boyadjiev, et al., J. Therm. Anal. Calorim. **137**, 1249 (2019). https://doi.org/10.1007/s10973-019-08030-0
38. Z. Y. Zhang, X. H. Li, C. H. Wang, et al., J. Phys. Chem. C **113**, 19397 (2009). https://doi.org/10.1021/jp9070373
39. C. R. Cena, M. J. Silva, L. F. Malmonge, et al., J. Polym. Res. **25**, 238 (2018). https://doi.org/10.1007/s10965-018-1633-0
40. A. Khan, A. M. Toufiq, F. Tariq, et al., Mater. Res. Express **6**, 065043 (2019). https://doi.org/10.1088/2053-1591/ab0aaf